Multi-Gain-Stage InGaAs Avalanche Photodiode with Enhanced Gain and Reduced Excess Noise

George M. Williams, Madison Compton, David A. Ramirez, Majeed M. Hayat, and Andrew S. Huntington

***Abstract*—We report the design, fabrication, and test of an InGaAs avalanche photodiode (APD) for 950–1650 nm wavelength sensing applications. The APD is grown by molecular beam epitaxy on InP substrates from lattice-matched InGaAs and InAlAs alloys. Avalanche multiplication inside the APD occurs in a series of asymmetric gain stages whose layer ordering acts to enhance the rate of electron-initiated impact ionization and to suppress the rate of hole-initiated ionization when operated at low gain. The multiplication stages are cascaded in series, interposed with carrier relaxation layers in which the electric field is low, preventing avalanche feedback between stages. These measures result in much lower excess multiplication noise and stable linear-mode operation at much higher avalanche gain than is characteristic of APDs fabricated from the same semiconductor alloys in bulk. The noise suppression mechanism is analyzed by simulations of impact ionization spatial distribution and gain statistics, and measurements on APDs implementing the design are presented. The devices employing this design are demonstrated to operate at linear-mode gain in excess of 6 000 without avalanche breakdown. Excess noise characterized by an effective impact ionization rate ratio below 0.04 were measured at gains over 1 000.**

***Index Terms*—Avalanche photodiode, optical receiver, photo detector, photon counting.**

I. Introduction

LINEAR-MODE avalanche photodiodes (APDs) are used in optical receivers for applications such as optical communications and laser radar, which benefit from the APD's internal photocurrent gain, fast response, compact size, durability, and low cost. A linear-mode APD's gain improves the signal-to-noise ratio of a photo receiver by boosting the signal photocurrent relative to circuit noise sources downstream in the signal chain.

The slope of an APD's gain curve as a function of reverse bias limits the gain at which it can be used. The slope of the gain curve is an issue because avalanche gain (M_{DC}) increases asymptotically in the vicinity of the APD's breakdown voltage (V_{br}) according to the empirical relation

$$M_{DC} = \left[1 - V/V_{br}\right]^{-n} \tag{1}$$

which holds for all APDs in which both carrier types (electrons and holes) can initiate impact ionization [1]. In (1), the parameter n controls how quickly the avalanche gain rises as V approaches its vertical asymptote at V_{br}; stable operation of APDs characterized by large values of n becomes impractical at high gains because V/V_{br} cannot be adequately controlled.

Avalanche noise imposes a separate limit on the useable gain of an APD. In the limit of high avalanche gain, the sensitivity of a hypothetical photoreceiver employing an ideal "noiseless" APD is limited by the shot noise on the optical signal itself. However, most APDs generate multiplication noise in excess of the shot noise already present on the optical signal; this excess multiplication noise intensifies with increasing avalanche gain, such that for any given level of downstream amplifier noise, there is a limit to how much avalanche gain is useful. Increasing the avalanche gain beyond the optimal value increases the shot noise faster than the amplified signal photocurrent, degrading the signal-to-noise ratio.

Excess multiplication noise results from the stochastic nature of the impact ionization process that amplifies the APD's primary photocurrent. For most linear-mode APDs, the gain distribution is that derived by McIntyre [2]. McIntyre's distribution is far from Gaussian for small inputs (i.e., for a small number of primary photocarriers injected into the multiplier), with a pronounced positive skew. For larger inputs, the McIntyre distribution approaches Gaussian due to the central limit theorem, and avalanche noise can be quantified for analysis with other common circuit noise sources by computing the variance of the gain. The Burgess variance theorem [3], [4] gives the variance of the multiplied output n for a primary carriers generated by a Poisson process and injected into a multiplier characterized by a mean gain M_{DC} and random gain variable m [5]:

$$\mathrm{var}(n) = M_{DC}^2 \mathrm{var}(a) + \langle a \rangle \, \mathrm{var}(m) = M_{DC}^2 F \langle a \rangle \tag{2}$$

where the excess noise factor F is defined as

$$F \equiv \langle m^2 \rangle / M_{DC}^2. \tag{3}$$

Manuscript received October 22, 2012; revised January 2, 2013, February 11, 2013, and March 7, 2013; accepted March 26, 2013. Date of publication April 29, 2013; date of current version June 13, 2013. The review of this paper was arranged by Editor A. G. Unil Perera.

G. M. Williams, M. Compton, and A. S. Huntington are with Voxtel Inc., Beaverton, OR 97006 USA (e-mail: georgew@voxtel-inc.com; madisonc@voxtel-inc.com; andrewh@voxtel-inc.com).

D. A. Ramirez and M. M. Hayat are with the Center for High Technology Materials, University of New Mexico, Albuquerque, NM 87106 USA (e-mail: davramir@unm.edu; hayat@chtm.unm.edu).

Color versions of one or more of the figures in this paper are available online at http://ieeexplore.ieee.org.

Digital Object Identifier 10.1109/JEDS.2013.2258072

2168-6734/$31.00 © 2013 IEEE

For most linear-mode APDs, the excess noise factor has the gain-dependence derived by McIntyre for uniform junctions [6]

$$F = M_{DC}\left[1-(1-k)\left(\frac{M_{DC-1}}{M_{DC}}\right)^2\right]. \tag{4}$$

In (4), the parameter k is the ratio of the hole-to-electron impact ionization rates. When $k > 0$, k is the slope of the excess noise curve as a function of gain, in the limit of high gain. For single-carrier multiplication, $k = 0$, and $F \rightarrow 2$ in the limit of high gain. Another feature of single-carrier ($k = 0$) multiplication is that avalanche breakdown cannot occur. Without participation of one carrier type, all impact ionization chains must eventually self-terminate, because all carriers of the type capable of initiating impact ionization soon exit the multiplying junction. The gain curve of a $k = 0$ APD does not exhibit the vertical asymptote described by (1), enabling stable operation at higher gain than a $k > 0$ APD.

Important exceptions to the excess noise factor formula (4) include APDs in which the carrier dead space is a significant portion of the width of the multiplying junction [7]–[10], those in which a change in alloy composition modulates the impact ionization threshold energy and rate across the multiplying junction [11]–[16], and those made from semiconductor alloys with band structures that combine the traits of single-carrier-dominated multiplication ($k \sim 0$) with an abrupt carrier dead space, resulting in correlation between successive impact ionization events [17]–[22]. The cascaded multiplier design presented here applies similar physics to achieve high-gain operation with low excess multiplication noise.

II. Reducing APD Multiplication Noise

The goal of impact ionization engineering (I^2E) is to reduce excess multiplication noise by designing semiconductor structures in which certain impact ionization chains that contribute to the gain distribution of a bulk multiplier have been eliminated, narrowing the engineered multiplier's gain distribution [23]. In general, I^2E designs use two tools: (a) the "dead-space" effect [24], and (b) localized enhancement of the ionization rate. Both reduce the number of possible ionization chains–and, hence, narrow the distribution of the multiplication gain–through spatial localization of the ionization events. Although I^2E APDs have been reported with k ~ 0 at very low gain, they have not been able to sustain this level of performance much above a gain of $M_{DC} \sim 4$.

Dead space is the physical displacement of an electron or hole inside an electric field required to pick up sufficient kinetic energy to trigger impact ionization. Secondary electrons and holes that are generated by impact ionization start out with little kinetic energy, and must pick up energy from the field in an APD junction before they can impact-ionize and generate progeny carriers. An APD designer can manipulate the dead space inside an APD junction to prevent impact ionization in certain regions, thereby affecting the gain statistics [25]–[28]. If the APD's gain distribution is truncated by using dead space to eliminate the longer impact ionization chains, its multiplication noise will be lower. However, absent the longer impact ionization chains, the APD's mean gain is also reduced.

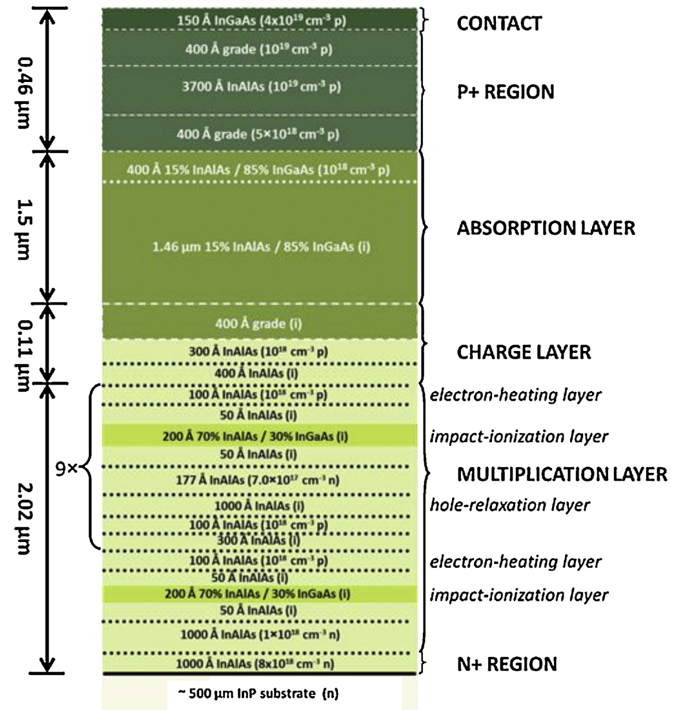

Fig. 1. Epitaxial layer structure of an SCM APD with 10 gain stages.

A change in semiconductor alloy composition inside the APD junction will result in a change of both the impact ionization threshold energy and the impact ionization rate, narrowing the gain distribution by making impact ionization much more likely in some locations and much less likely in others [13], [29]. However, like APDs that employ dead-space effects, the spatial localization of impact ionization reduces the number of possible ionization chains and can result in reduced mean avalanche gain.

Higher gain can be obtained from a thin multiplication layer by increasing the field strength, but in doing so, feedback from hole-initiated ionizations is intensified and noise suppression is lost, precisely because longer ionization chains can now fit into the same space. Not only do stronger fields degrade excess noise performance, they increase dark current leakage by band-to-band and trap-assisted tunneling, which limits the gain over which thin-multiplier designs are effective.

III. Single Carrier Multiplication Avalanche Photodiodes

A. *Single Carrier Multiplication Avalanche Photodiode (SCM APD) Architecture*

The multi-stage single carrier multiplication (SCM) APD was developed for low noise, high gain operation [30]. The SCM APD applies the traditional I^2E techniques of dead-space and alloy selection with tailoring of the electric field profile to modulate impact ionization probability. To achieve high gain and low excess noise simultaneously, SCM APDs are designed using J cascaded asymmetric multiplication regions (Fig. 1).

Each hetrostructured gain stage is designed for low excess noise at low gains (i.e., $< m_j >$ less than 2). By cascading gain

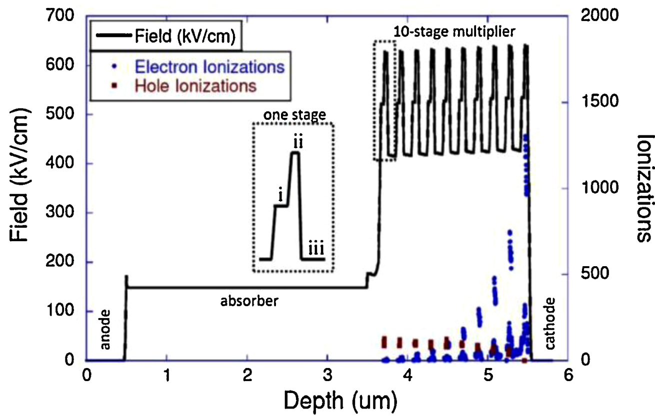

Fig. 2. Spatial distribution of electron- and hole-initiated impact ionization (points) plotted against electric field profile for 100 samples of a 20 000-trial Monte Carlo simulation of a 10-stage SCM APD operating at a mean gain of M_{DC}= 600. An excess noise of $F(M_{DC})$ = 6.47 was simulated.

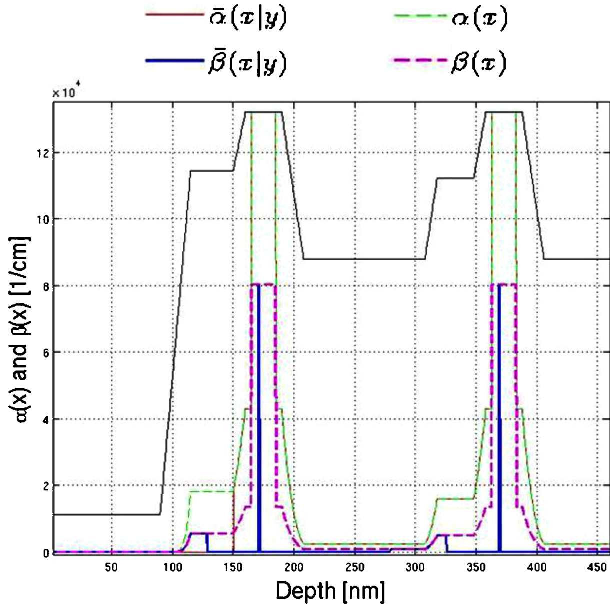

Fig. 3. Impact ionization coefficients for electrons, α, and holes, β, across the structure by considering phonon scattering (solid curves) and by neglecting phonon scattering (dashed curves) for M_{DC} = 937 bias conditions. The plot is a zoomed view of the impact ionization in two stages.

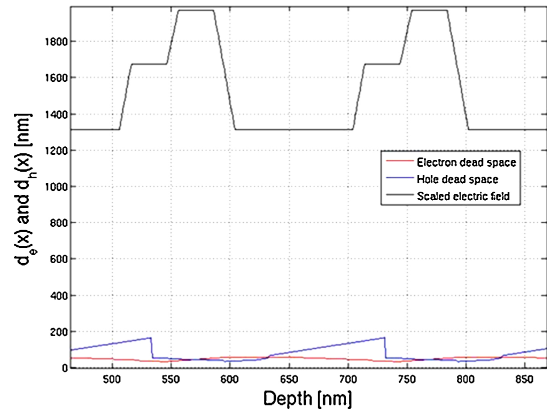

Fig. 4. Dead-space profile of electrons and holes in a two gain stage region of the SCM APD multiplication region. Shown for reference is a plot of the electric field (arbitrary units).

stages in the multiplication region, high overall net gain can be achieved while preserving the low excess noise of each gain stage. For example, neglecting any gain resulting from ionization feedback, if a low noise gain region with an effective mean gain of $<m_j> = 1.7$ is cascaded in a series of five equivalent gain stages, a net gain of $M_{DC} = 14$ is achieved; a seven-stage device achieves a gain of approximately $M_{DC} = 41$; and a ten-stage device reaches a gain of about $M_{DC} = 202$.

The SCM APD's cascaded multiplier design [31] is conceptually similar to the "staircase" APD described by Williams *et al.* in 1982 [32], but does not rely upon band-edge discontinuities at hetero-interfaces to manipulate carrier energy. Instead, doping is used to modulate the electric field inside the multiplying junction, which modulates carrier energy by either accelerating carriers in high-field regions or allowing hot carriers to thermalize in regions of low electric field strength; alloy composition is varied to pattern the impact ionization threshold energy. These techniques are applied to reduce the randomness of the multiplication process by suppressing hole-initiated ionizations and enhancing electron-initiated ionizations, while also spatially localizing the latter. Electron-only multiplication eliminates all the impact ionization chains involving hole avalanche from the universe of possible gain processes, significantly narrowing the gain distribution. Restricting impact ionization to small regions of the junction likewise eliminates certain gain processes that would otherwise contribute to gain variability. Thus, the cascaded multiplier design suppresses excess multiplication noise by physically eliminating many of the gain processes that contribute to gain variability.

Within each gain stage, the asymmetric electric field profile is responsible for suppressing hole-initiated impact ionization. Carriers impact-ionize most readily in the AlGaInAs layer which combines a lower impact-ionization threshold with the highest electric field strength. However, the impact ionization layer is sized to be approximately the carrier dead space, meaning that carriers that are injected into that layer cold are unlikely to pick up sufficient energy to ionize before exiting the layer. The electric field profile is patterned so that electrons are pre-heated prior to injection into the impact ionization layer, whereas holes are injected cold.

This structure would not achieve noise suppression if the holes were to pick up kinetic energy in one gain stage and enter into an adjacent stage with sufficient energy to impact-ionize. Therefore, the gain stages are separated by low-field carrier relaxation regions in which both electrons and holes lose their accumulated kinetic energy through random phonon scattering. In this way, the holes generated in later gain stages drift back through the earlier gain stages, to the anode, without impact ionizing.

B. SCM APD Device Simulation

1) *Monte Carlo Models of SCM APD:* To develop the multi-stage APD design, and to aid in the design of the SCM APD, a quasi-empirical Monte Carlo simulator of impact ionization in arbitrary junction designs was written. The Monte

Carlo simulator treats material- and field-dependent variation in ionization threshold energy and ionization rates, and tracks carrier energy effects such as dead space and relaxation. It is quasi-empirical in the sense that it does not directly calculate scattering rates, relying instead upon simple field-dependent exponential models of the impact-ionization rate of active carriers, impact-ionization threshold energies, and estimates of carrier mean free path published by others. A recursive algorithm is used to simulate ionization chains.

Fig. 2 plots the spatial occurrence and number of hole- and electron-initiated impact ionization events from a 100-trial subset of a 20 000-trial simulation of a 10-stage SCM APD operating at an average gain of $M_{DC} = 599$.

It should be remarked that the electric field profile found by the band edge simulator is based on an idealization of the dopant distribution in which doping concentration is uniform, and doping is confined to the epitaxial layers into which the dopant species were introduced during growth.

In Fig. 2, electrons drift from left to right, from anode to cathode, and holes drift from right to left; photo carrier pairs are initially generated in the APD's InGaAs absorber such that only photoelectrons are injected into the multiplier. As shown in the inset in Fig. 2, the purpose of the first layer of one of the repeating asymmetric gain stages (labeled "i") is to pre-heat electrons prior to injection into the impact-ionization layer (labeled "ii"), while keeping the electric field low enough that holes exiting the impact-ionization layer are unlikely to ionize. The impact-ionization layer (labeled "ii") is characterized by both a higher field and a semiconductor material ($Al_{0.335}Ga_{0.140}In_{0.525}As$) with a smaller bandgap (1.20 eV versus 1.46 eV) than the surrounding $In_{0.521}Al_{0.479}As$. The combination of a strong electric field and a lower impact-ionization threshold energy in layer (ii) promotes impact-ionization by hot electrons injected from layer (i), but the layer is designed to be too thin for the cold holes injected from the energy relaxation layer (labeled "iii") to pick up sufficient energy to ionize. Finally, layer (iii), is characterized by an electric field sufficiently low that individual hole carriers spend very little time with kinetic energy in excess of the ionization threshold; this suppresses the probability of hole ionization, so that low noise avalanche multiplication is achieved [30].

Carriers traveling at the saturation drift velocity are expected to have mean kinetic energy on the order of the optical phonon energy of 30 – 40 meV, whereas the impact-ionization threshold energy is about 1 eV in InGaAs or 2 eV in InAlAs. Within region (iii) the impact-ionization rate is negligible because the mean free path between phonon collisions is short compared to the displacement in the field required to accumulate the impact-ionization threshold energy, such that individual carriers spend very little time with kinetic energy in excess of the ionization threshold. In contrast, at the electric field strength characteristic of the impact-ionization layer, carriers have a reasonable probability of accumulating the threshold energy so that they ionize before losing energy through scattering. Thus, the function of region (iii) is to reset the dead space of active carriers exiting impact-ionization layers while minimizing the likelihood those active carriers will impact-ionize before scattering; this helps localize the avalanche to the impact-ionization layers and prevents injection of active holes into impact-ionization layers.

TABLE I

MATERIAL PARAMETERS TO CALCULATE THE IMPACT IONIZATION RATES; α, $\beta = A\exp[-(B/E_{field})^m]$

Material	A (cm^{-1})	B (V/cm)	m	Carrier
InGaAs	1.8*10^7	1.95*10^6	1	Electrons
	2.56*10^7	2.2*10^6	1	Holes
InAlAs	4.17*10^6	2.09*10^6	1.2	Electrons
	2.65*10^6	2.79*10^6	1.07	Holes

TABLE II

THRESHOLD ENERGIES USED TO CALCULATE THE DEAD-SPACE PROFILE

Material	Threshold Energy (eV)	Carrier
InGaAs	1.20	Electrons
	1.00	Holes
InAlAs	2.15	Electrons
	2.30	Holes

For the specific simulation of the 10-stage SCM APD biased for $M_{DC} = 599$ presented in Fig. 2, the Monte Carlo model predicted an excess noise factor of $F = 6.47$, which, using (9) is equivalent to a bulk multiplier with an effective ratio of hole-to-electron ionization rate of $k \sim 0.007$. Good agreement between modeled and measured results has been obtained over a number of different designs, gain stages, and operating biases. However, the limitations of implementation and approximation should be recognized. The device structure analyzed by the Monte Carlo model is an idealization of what can be grown epitaxially. The use of a hard dead space, a fixed energy relaxation length, and impact-ionization rates for active carriers that are independent of carrier energy are all simplifying assumptions. As such, the Monte Carlo model was useful for designing the SCM APD and interpreting measurements on SCM APDs, although it uses empirical parameters to obtain accurate results, so it ought not be regarded as quantitatively predictive as a full-band Monte Carlo model.

2) *Dead-space Multiplication Theory (DSMT) Numeric Models of SCM APD:* To validate Voxtel's Monte Carlo model, University of New Mexico (UNM) authors, using the same impact ionization threshold energies and field-dependent rate models as used in the Voxtel simulation, performed numeric simulations. The purpose of the UNM calculations was to analyze the SCM APD design by a separate methodology. Table I summarizes the parameters used by both models to calculate the field-dependent impact ionization rates for active carriers (i.e., those with kinetic energy in excess of the impact ionization threshold), taken from Saleh *et al.* [33]–[34] and Pearsall [35].

The pre-factors, A, for InGaAs were reduced by a factor of 2.85 from those published by Pearsall to fit the Monte Carlo model's calculation of excess noise factor to the measurements for the I^2E structure reported by Wang *et al.* [13]. This was done because the authors of this paper are unaware of any impact-ionization rate models published in the literature for the quaternary alloy $Al_{0.335}Ga_{0.140}In_{0.525}As$ used in the SCM APD

multiplier. However, the excess noise data published by Wang *et al.* is for an I^2E APD that uses the same alloy composition. The quaternary alloy is implemented as a blend of the lattice-matched ternary alloys $In_{0.52}Al_{0.48}As$ and $In_{0.53}Ga_{0.47}As$, so ionization coefficients for the quaternary AlGaInAs alloy were estimated as the appropriate linear combination of the ionization coefficients for the lattice-matched ternary alloys. The 2.85 magnitude reduction of the pre-factors is within the range of ambiguity for $In_{0.53}Ga_{0.47}As$ found by Osaka *et al.* [36] who remark that Pearsall's rate coefficients for InGaAs are approximately one order of magnitude greater than those they measured.

Table II lists the threshold energies used to calculate the dead space, also taken from Saleh *et al.*

To accommodate for carrier relaxation due to phonon scattering, the nonlocalized ionization coefficients have been modified in this paper to a new kind of ionization coefficients, which we call the "scattering-aware" ionization coefficients, which we integrated into a recursive dead-space multiplication theory (DSMT) impact ionization model [12], [37] to capture carrier "reset" effects. Once these scattering-aware ionization coefficients are calculated, they are substituted for the nonlocalized ionization coefficients in the expression for the probability density function (PDF) of the distance to the first ionization.

a) *Notion of Scattering-aware Ionization Coefficients:* The model for the PDF of the distance to the first impact ionization has been modified to incorporate a relaxation mechanism for suppressing the impact ionizations triggered by one species of carrier, such as through phonon scattering. Specifically, we assume that a carrier loses its energy and ceases to be able to impact-ionize if it travels a certain nominal distance during which the electric field is below a certain threshold (30 nm below 10^3 V/cm in our studies) [38]. More precisely, we shall assume that the energy accumulated by a carrier is reset to zero once the carrier travels the nominal distance under a field that falls below a certain threshold.

The scattering-aware ionization coefficient for holes and electrons, $\bar{\alpha}(y|x)$ and $\bar{\beta}(y|x)$, respectively, are defined as follows: $\bar{\alpha}(y|x)$ is the ionization coefficient at y for an electron that has zero energy at location x, with $x < y$, and $\bar{\beta}(y|x)$ is the ionization coefficient at y for a hole that has zero energy at location x, with $x > y$. Note that unlike the nonlocalized ionization coefficients, these coefficients are dependent on the entire field profile from x to y, not just on the field at y. The scattering-aware ionization coefficients are calculated as follows: Let $d_e(x)$ and $d_h(x)$ denote the dead spaces that an electron and hole, respectively, created at location x in the multiplication region must travel before they can accumulate their ionization threshold energy in the material. For an electron starting at location x with zero energy reserve, we set $\bar{\alpha}(y|x) = 0$ if $y < x + d_e(x)$. However, if $y \geq x + d_e(x)$, then we find the last point, s, at which the energy of the electron was reset to zero, and then check whether the electron has traveled the dead space $d_e(s)$ beyond the point s. If indeed it has traveled $d_e(s)$ beyond s, we set $\bar{\alpha}(y|x) = \alpha(y)$, where $\alpha(y)$ is the usual nonlocalized ionization coefficient (also termed enabled ionization coefficient in [2]). On the other hand, if it has not travelled a distance $d_e(s)$ beyond s, we set $\bar{\alpha}(y|x) = 0$. The scattering-aware ionization coefficient for the holes is calculated similarly. Once the scattering-aware ionization coefficients are calculated, they are substituted for the nonlocalized ionization coefficients in the expression for the PDF of the distance to the first ionization using the shifted exponential PDF used by the DSMT [1]. The scattering-aware PDFs for $y \geq x$, are given by

$$h_e(y|x) = \begin{Bmatrix} \bar{a}(y|x)\exp\left(-\int_{x+d_e(x)}^{y} \bar{a}(z|x)dz\right)_{,w\geq y\geq x+d_e(x)} \\ 0, \quad 0<y<x+d_e(x) \end{Bmatrix} \tag{5}$$

and for $y < x$, are given by

$$h_h(y|x) = \begin{Bmatrix} \bar{\beta}(y|x)\exp\left(-\int_{y}^{x-d_h(x)} \beta(z|x)dz\right), \quad 0\leq y\leq x-d_h(x) \\ 0, x\geq y>x-d_h(x) \end{Bmatrix}. \tag{6}$$

Note that the scattering-aware ionization coefficients capture scattering in a more detailed manner than that captured by the "bulk" (localized) as well as enabled and history-dependent ionization coefficients. This is because the scattering-aware coefficients track the history of the electric field experienced by a carrier as it is transported. For example, while the nonlocalized ionization coefficient obtained by fitting the DSMT to experimental F vs. M_{DC} data [34] can capture scattering effects statistically, the scattering-aware coefficients have the added feature of actively resetting the energy of carriers as they are transported, which is more suitable for layered multiplication regions where the location of high and low scattering is controlled in space by means of changing the electric field.

b) *Scattering-aware DSMT Applied to SCM APD Design:* Fig. 2 shows the nonlocalized and scattering-aware ionization coefficients for electrons, α, and holes, β, across the structure. The dashed lines represent the case in which phonon scattering is neglected, while the solid lines represent the case in which phonon scattering is considered. Including phonon scattering in the numerical models results in a tighter spatial distribution of electron ionization events in each gain stage, while reducing the occurrence of hole ionization events throughout the structure. When the phonon scattering in the energy relaxation region (Fig. 2, inset "iii") is taken into consideration, the numeric models show that electrons ionize almost immediately upon entering the high electric field region of the impact-ionization layer (Fig. 2, inset "ii"), but have a low probability of ionizing elsewhere in the gain stage. When phonon scattering is considered, the hole ionization rate is negligible throughout the entire gain stage. The "scattering-aware" ionization rates more closely resemble the Monte Carlo plots of Fig. 2, whereas the models that do not include phonon scattering have ionization rates of larger magnitude and wider spatial extent for both holes and electrons.

Fig. 4, shows the dead-space profile calculated for electrons and holes taking into account phonon scattering effects over a few periods of a 10-stage SCM APD multiplier. The excess

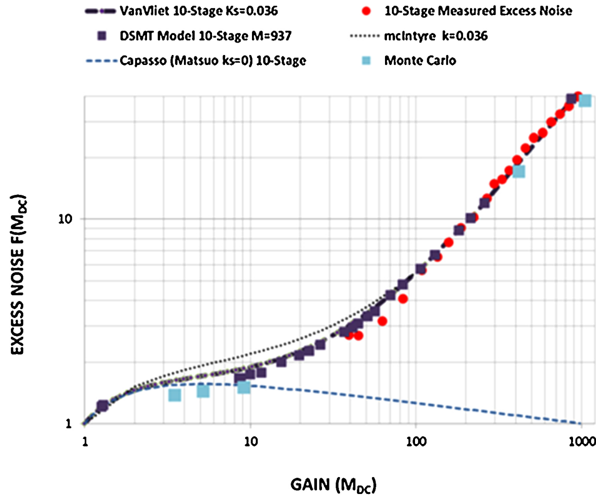

Fig. 5. Plots of excess noise predicted by the DSMT numeric model for a 10-stage SCM-APD operated at a $M_{DC} = 937$ bias and the Monte Carlo modeled results ($M_{DC} = 1200$) compared to measured excess noise data for a 10-stage SCM-APD ($M_{DC} = 1200$). Also plotted are: the McIntyre model (4; k = 0.36), the VanVliet model (9; $k_s = 0.036$) for a two-carrier ionization 10-stage SCM APD, and the Capasso model (8) for an ideal 10-stage device.

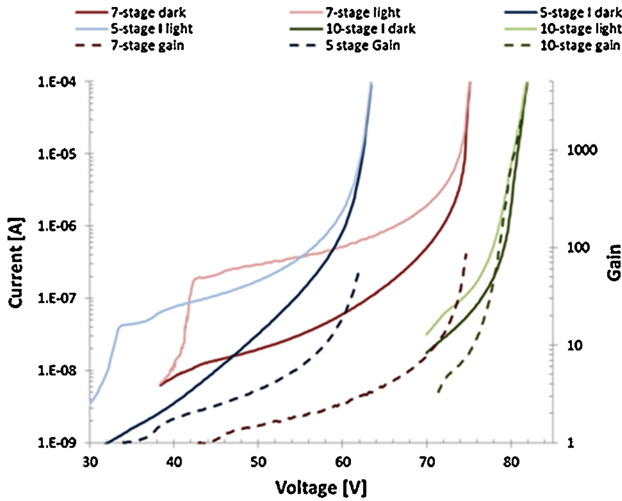

Fig. 6. Measured I-V and Gain Curves for 5-, 7-, and 10-stage SCM-APD devices, taken at 300 K. The light levels are chosen so that the noise is dominated by the statistics of the photocurrent, but does not saturate the detector at the highest gain bias settings. For the 10-stage device, four different light levels were used so that good signal to noise was achieved in the measurements. Only the lowest light level, which didn't saturate the detector over the full range of biases, is shown. Notably, the 10-stage device did not exhibit breakdown behavior.

noise-gain characteristics predicted by the DSMT for a 10-gain-stage SCM APD are shown in Fig. 5. The DSMT and Monte Carlo models of Fig. 5 predict similar performance and are in good agreement with the empirically measured results. Also plotted in Fig. 5 are the analytical McIntyre-modeled excess noise values from (4; $k = 0.036$). It is to be expected, at most biases, that the empirical and numerically modeled results do not match (4) as the SCM-APD design differs from that of a bulk, dead-space free APD assumed by McIntyre [2]. The data converge with the McIntyre formula only at DC gain levels above about 125.

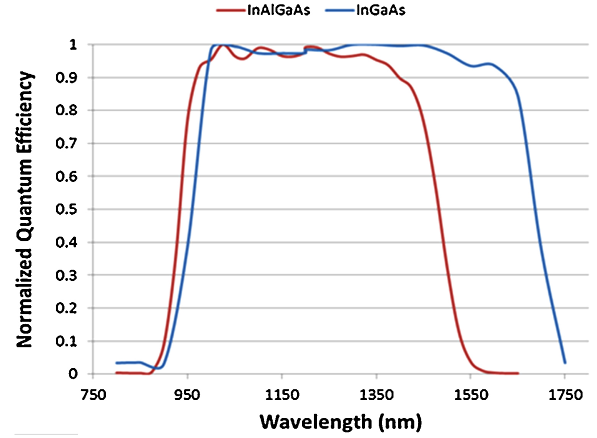

Fig. 7. Normalized quantum efficiency (QE) measurements for the InGaAs (5- and 7- stage) and InAlGaAs (10-stage) SCM APDs.

3) *Analytical Discrete Low-Gain Multi-Layer APD Models:* For an ideal SCM APD device without hole feedback, $F(M_{DC})$ can be expressed in terms of the electron count mean and variance that results from a single primary relation event, and the excess noise factor is only due to those carriers that cannot ionize, δ, where $\delta = 1 - P_e$ and P_e is the probability that the electron ionizes in each gain stage. In this specialized case, the gain is

$$M_{DC} = (2 - \delta)^J, \tag{7}$$

where J is the number of gain stages. With only single-carrier ionization, the excess noise factor after Capasso [39] is

$$F(J, \delta) = 1 + \frac{\delta[1 - (2 - \delta)^{-J}]}{(2 - \delta)}. \tag{8}$$

Note that in (8) $F(J, \delta)$ is < 2 for any J. When $P = 1$, in the absence of carrier fluctuations, $var(J, \delta) = \delta(1\text{-}\delta) = 0$ and $F = 1.0$. This cannot be achieved in a conventional APD at high gain even if one of the ionization coefficients is zero. However, these conditions may apply to the SCM APD at low biases, assuming there is not significant hole ionization feedback.

Assuming two carrier ionization multiplication processes, in a low-gain limit, the discrete nature of the ionization process for both carriers must be taken into account. This has been analyzed by Van Vliet [40] and by Lukaszek [41] and leads to a lowering of the excess noise factor, compared to McIntyre predictions, for sufficiently low gains. When both hole- and electron-ionization are included in a multi-stage discretized APD, the excess noise can be approximated after [40], [42] as

$$\begin{aligned} F(J, \delta) = 1 + \frac{\left(1 - 1/_{<M_{DC}>}\right)^{(1-k_s)}}{2 + P(1-k_s)} * \\ \left[-P + 2\frac{(1-k_s P^2)}{(1+k_s P)}\left(\langle M_{DC}\rangle\, k_s \frac{(1+P)}{(1-k_s)} + \frac{1}{1+P}\right)\right], \end{aligned} \tag{9}$$

where $k_s = Q/P$ is the ratio of the hole-ionization probability per gain stage, Q, to the electron-ionization probability per gain stage P, and the mean output gain, $<M_{DC}>$, is calculated by

$$M_{DC}(J) = \frac{(1 + P)^J (1 - k_s)}{(1 + k_s P)^{J+1} - k_s (1 + P)^{J+1}}. \tag{10}$$

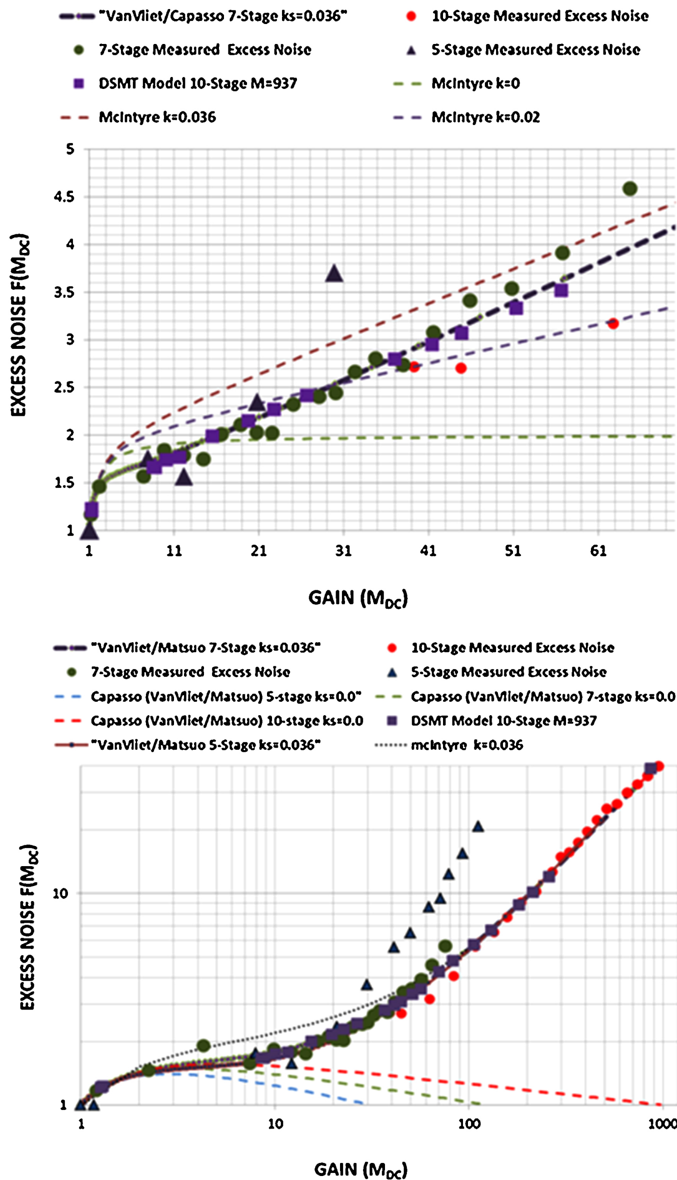

Fig. 8. Plots of excess noise measurements for the 5-, 7-, and 10-stage SCM APDs plotted on a linear scale for the gains below 70 (TOP) and on a log-log scale for the entire gain range (BOTTOM). Also plotted is the DSMT numerically modeled data (10-stage SCM APD with M_{DC} = 937), a VanVliet model (9) of a 7-stage device with k_s = 0.036, and McIntyre (4; k = 0, 0.2, and 0.036) predicted performance. In the bottom plot, the measured data are shown with the Capasso model (8) for an ideal 5-, 7-, and 10-stage SCM-APD, the VanVliet (9; k_s= 0.036) and McIntyre (4; k = 0.036) models.

The van Vliet model (9; $k_s = 0.036$) is plotted in Fig. 5 as a function of gains calculated by (10; $k_s = 0.036$) over all possible values of P. The analytical models show good agreement with the Monte Carlo and DSMT simulations over most bias conditions, and approximate the McIntyre models only at higher biases (i.e., $M_{DC} > 125$).

The agreement between (9) and the numeric DSMT simulations is not surprising, as it has been shown previously that an SCM APD with dead space can be approximated by a superlattice (ideal, discrete multilayer) APD for which the separation between the layers is the dead space, and the ionization probability per layer is obtained by matching the gains of the two devices [43]. However, unlike the analytical excess noise models (4) and (9), the DSMT does not involve any fitting parameters (i.e., k and k_s) to the data; it only uses universal parameters for the nonlocalized ionization coefficients, the materials' ionization threshold energies, and simple phonon-scattering rules.

IV. SCM APD Device Design and Fabrication

A. SCM APD Epitaxial Growth

SCM APDs with the multiplier design presented in Fig. 1 were grown by MBE on 2" n-type (100)-oriented InP substrates. Three-, 5-, 6-, 7- and 10-stage SCM APDs were grown with $Al_{0.07}Ga_{0.40}In_{0.53}As$ absorbers; 7-stage SCM APDs were grown with $In_{0.53}Ga_{0.47}As$ absorbers.

Physical implementation of this design requires that the p- and n-type doping within each multiplying stage balance nearly quantitatively. A net excess of space charge in the multiplier effectively adds to or subtracts from the doping of the charge or "field control" layer, which changes the punch-through voltage of the APD, causing either early punch-through with tunnel leakage in the absorber or late punch-through and breakdown without photosensitivity.

Dopant cell flux, growth temperature, and growth rate tend to be very consistent for adjacent epitaxial layers in a single MBE growth run, so doping errors during SCM APD multiplier growth are systematic rather than random. The doping precision required to balance SCM APD multipliers cannot always be achieved by routine methods such as Hall effect measurement of doping calibration samples, so a series of SCM APD wafers are normally grown in which the thickness of the n-type layer is incrementally varied relative to a constant p-type layer specification. This method, aided by the systematic nature of the doping mismatch, generally achieves good results.

B. Device Fabrication

Back-illuminated photodiodes of varying diameter were etched in the molecular beam epitaxy (MBE) -grown epitaxial material. Anode pixel contacts on top of the diode mesas and annular cathode contacts at the base of the mesas were patterned, and following a cleanup etch to remove surface material contaminated by the contact metallization and rapid thermal anneal, the mesa sidewalls were encapsulated with a polymer. A two-layer broadband anti-reflection coating was applied to the backside of the InP substrates after polishing.

V. Experimental Results

A. Test Procedures

Gain curves were generated from the current-voltage (I-V) characteristics of the APDs. Initial I-V screening was performed by needle-probing APDs on-wafer; later, individual packaged parts were fixtured and tested. In either case, an HP 4155A semiconductor parameter analyzer was used to sweep applied reverse bias and read the current. Stable, switchable illumination was projected onto the detector under test (DUT) by either a light-emitting diode (for on-wafer testing) or an OZ Optics OZ-2000 stabilized fiber-coupled 1064 nm diode

laser (testing of packaged components). Room temperature on-wafer testing was performed in a dark box housing a probe station. The packaged parts were tested inside a vacuum cryochamber.

Following burn-in under bias, during which the APD's I-V characteristics stabilized, light and dark I-V and capacitance-voltage (CV) curves were measured at 300K. The dark current was measured directly, and the avalanche gain of the photocurrent was calculated using

$$M(V) = \frac{I_{light}(V) - I_{dark}(V)}{I_{light}(V_{M=1}) - I_{dark}(V_{M=1})}. \tag{11}$$

In (11), $V_{M=1}$ is the unity-gain reference point. Correct identification of $V_{M=1}$ is critical to the scaling of both gain and excess noise data, as it is important to measure photocurrent and noise power levels relative to their unity gain values.

In InGaAs APDs, the depleted volume from which the multiplying junction collects primary carriers initially grows with reverse bias. Maximum collection of primary photocarriers normally occurs just after "punch-through," which is the bias at which the growing depletion region penetrates the charge layer interposed between the multiplication layer and the narrow-gap absorber to which photocarrier generation is confined. The unity-gain condition is normally identifiable as a plateau in the photocurrent immediately after punch-through, where collection of primary photocarriers is at a maximum, but before the impact-ionization process has turned on in the multiplier. However, if a narrow-gap cap layer is used to promote an ohmic contact, then a second source of photocarriers may be present in a top-illuminated structure. Photocarrier collection will continue to grow slightly as the depletion layer expands into the absorber, overlapping with the diffusion tail of photogenerated carriers from the cap. This can lead to a small double-plateau in the measured photocurrent, and incorrect scaling of gain and noise data if $V_{M=1}$ is chosen before the second plateau. In other cases, an APD's multiplier will already be operating above unity gain by the time maximum photocarrier collection is achieved. In this case, the unity-gain reference photocurrent cannot be measured directly, and the scaling of gain and noise measurements will be less accurate. In such cases, measurement of spectral responsivity can help estimate the gain at punch-through, based on the quantum efficiency expected of the absorber design.

Room temperature excess noise measurements were performed on ceramic submount-packaged APDs fixtured inside a dark box. Bias was applied to the contacts of the sub-mounted APDs using an HP 4155A semiconductor parameter analyzer (SPA) and a Cascade Microtech model ACP8U-AW-GSG-150 microwave probe (50 Ω). In the excess noise test, a bias-T coupled the DC component of the diode current to the SPA, and sent the AC component to a Mini-Circuits ZX60-3018G-S low noise amplifier. The amplifier fed either a spectrum analyzer or a noise figure meter. In this way, both the average DC gain (M_{DC} – calculated in the usual way from the DC component of the photocurrent) and the noise power spectral intensity at a given frequency (S_P – from the AC component) were read simultaneously. An HP 8566B spectrum analyzer was used to select a handful of low environmental noise frequencies within the 30 to 100 MHz band, and an HP 8970B noise figure meter was used to make calibrated noise power measurements.

Noise power measurements were taken both in dark and under-illuminated conditions. The fiber delivered optical signals sub-filled the SCM APD active area, and, via a fiber splitter, the optical power level was monitored using a calibrated Newport model 8181G InGaAs reference and Newport 1830-C optical power meter.

By selecting a light level that generated photocurrent about 10x the level of the dark current, the noise power of the photocurrent was isolated from the noise power of the dark current, allowing the noise power of the dark current to be subtracted. To ensure that the optical source dominated noise performance, noise statistics were calculated at unity gain and every other bias used for testing, using a series of optical power levels. Calibrated responsivity measures were also taken during testing to confirm the signal gain and to detect any non-linear saturation effects.

The noise figure meter outputs noise power spectral intensity measurements (S_P in W/Hz), and the impedance of the test circuit must be found in order to convert these measurements to noise current spectral intensity (S_I in A^2/Hz). The noise measurement at unity gain was used for this normalization, rather than a measurement of the DUT's impedance in isolation, because this gives the most direct measurement of the relevant impedance. It includes effects from the mounting of the detector, its interaction with the preamplifier and noise figure meter, and anything specific to the frequency band used for the noise power measurement. The normalization was accomplished using Schottky's theorem, $S_I = 2qI$ [A^2/Hz], and direct measurement of the DC photocurrent (I):

$$R = S_P/S_I = S_P/(2qI) \tag{12}$$

Between 20 and 30 independent measurements of the light and dark noise power at unity gain were used to find R. Subsequently, noise current spectral intensity was measured at a variety of different values of M_{DC}, taking 10 independent measurements of light and dark noise power for each gain point. Finally, excess noise factor was calculated using the noise current spectral intensity theorem for avalanche multiplication using

$$S_I = 2qIM^2F(M_{DC}). \tag{13}$$

The effect of this methodology was to measure accurately the test circuit's impedance under the same conditions as the noise measurements so that the generated excess noise curve is normalized for $F(M_{DC}) = 1$ at $M_{DC} = 1$, so that the data satisfied Schottky's theorem.

However, there is always experimental variation associated with the noise power measurement, so this measurement of the test circuit impedance is not absolutely accurate. Accordingly, one generally finds some scatter in the $F(M_{DC})$ data at higher gain. This is an experimental limitation, which we minimized by averaging a large number of noise measurements, and by selecting relatively "quiet" RF frequency bands in which to make our measurement, but it cannot be eliminated entirely.

Calibration of the excess noise measurements is sensitive to identification of the point in the APD's I-V characteristic where full collection of primary photo carriers is reached, and the gain at that point. When full collection of primary photo carriers occurs at a reverse bias for which $M_{DC}>1$, (11) is no longer valid, and using (12) to estimate R requires that one assume a value for the APD's excess noise factor at the reference gain, which is problematic since R scales all of the noise power measurements that are subsequently used to measure the excess noise at higher gain. Because of the forms of (4) and (9), the excess noise factors at low gain are not especially sensitive to the value of k that is assumed. For instance, for $k = 0.3$ (bulk InAlAs) at $M_{DC} = 1.5$, $F = 1.38$, whereas for $k = 0.02$ (a good silicon APD) at $M_{DC} = 1.5$, $F = 1.34$. Thus, as a practical matter, the test system impedance calibration problems introduced by punch-through above unity gain are manageable so long as the gain at punch-through is low enough.

Potential errors were minimized by using the C-V measurements to confirm punch-through. The unity gain responsivity values were also compared to SCM APDs with the same absorption layer composition and thickness, albeit with a different number of gain stages, and it was verified that the devices' quantum efficiencies are within the range of previously manufactured APDs with similar absorption layers (i.e., 70 to 90 percent depending on composition and wavelength).

To achieve good signal-to-noise and to avoid saturation effects, gain measurements were taken at a number of light levels. The relative gain and excess noise at each bias were verified by fitting gain-normalized optical power spectral density curves to the unity gain (i.e.,"shot noise limited") measurement, which confirmed the consistency of the gain measurements. Gain was further confirmed by gain-normalized plots of the trap-assisted-tunneling dominated dark current to the activation energy of the traps.

The I-V curves for the various multi-gain stage devices are shown in Fig. 6. The onset of punch-through in the 5-stage device is quite evident, and using the responsivity measurements of the 5-stage AlGaInAs absorption layer device at unity gain, the gain of the 10-stage device, where the onset of punch-through occurs after unity gain can be determined more accurately.

Punch-through of the 7-stage InGaAs absorption layer APD is also evident and was further calibrated by comparing the unity gain responsivity (Fig. 7) to comparable thickness InGaAs absorption layer conventional SACM APDs fabricated using the same process.

VI. Measured SCM APD Noise Performance

In all, several hundred devices were tested, and excess noise measurements were performed on approximately 30 SCM APDs selected from different wafers manufactured on several lots. The devices were tested over the 77K to 295 K temperature range.

The 295 K excess noise measurements for the 5-stage, 7-stage, and 10-stage SCM APDs are shown as a function of mean gain in Fig. 8, wherein the low gain excess noise measurements are plotted on a linear scale, and the excess noise measurements over the full gain range of the SCM APDs is plotted on a log-log scale. Also plotted in Fig. 8 are: the numerically modeled data for a 10-stage SCM APD with an $M_{DC} = 937$ bias, McIntyre [i.e., (4; $k = 0$, 0.2, and 0.36)] -modeled data, VanVliet [i.e., (9; $k_s = 0.036$)] -modeled data for SCM APD, and the Capasso (8)-modeled data for ideal (no ionization feedback) 5-, 7-, and 10-stage SCM APDs.

VII. Discussion of Results

In Fig. 5, it was shown that the measured 10-stage SCM APD excess noise data matches that predicted by DSMT numeric models, the Monte Carlo models, and analytical discrete multilayer APD models [i.e., (9)]. The measured excess noise curves shown in Fig. 8 further bear out the design principles employed in the SCM APD design.

A. Gain and Excess Noise Performance

The excess noise data of Fig. 8 includes the performance of 5-, 7-, and 10-stage devices and provides further insight into the SCM APDs' noise properties and bias (electric field) -dependent carrier dynamics. There are five noise domains evident in the excess noise data.

1) *Single-carrier Dominated Multiplication:* At the lowest biases, a majority of the gain results from the current induced in the circuits by the initial photoelectron and the ionizing electron progeny as they traverse the gain stages during the photoelectron's transit of the multiplication region. Assuming minimal hole ionization feedback, the excess noise in this region can be characterized by the Capasso model (8). This region is best represented by the 7-stage SCM APD data in Fig. 8. The measured data appears to depart from (8) at about $M_{DC} = 50$, which, from (7), would suggest $P = 0.25$. From the fit of (9; $k_s = 0.036$) at higher biases, we can estimate the probability of hole ionization to be about $Q = 0.009$. The largest number of electron-hole pairs are created at the last gain stage, and given the $(J - 1)$ gain stages the holes can potentially ionize during their drift toward the $p+$ contact, there is an insufficient probability of feedback to sustain further avalanche. Thus, we can assume that a majority of the gain occurs during the initial transit time of the photoelectron.

2) *Discrete, Low Gain per Stage Multiplication:* As the device's operating bias is increased, P and Q increase proportional to k_s until Q is of a magnitude sufficient to sustain hole-ionization feedback. Under these bias conditions, both P and Q are still quite low, so the carrier multiplication in each gain stage is low; hence, the device may be approximated by the two-carrier discrete gain stage model (9). As can be seen in Fig. 8, the measured data can be approximated by (9; $k_s = 0.036$). In this bias range, the measured 7-stage and 10-stage SCM APD data are well below the McIntyre model (4; $k = 0.036$) of a "bulk" semiconductor multiplication region APD with no dead space.

To gain insight into the SCM APD carrier dynamics, the band edge modeler was used to estimate the electric field in each device as a function of bias. In Fig. 9, the estimated electric field curves are plotted along with the electron ionization probabilities estimated by (10) for the average gain

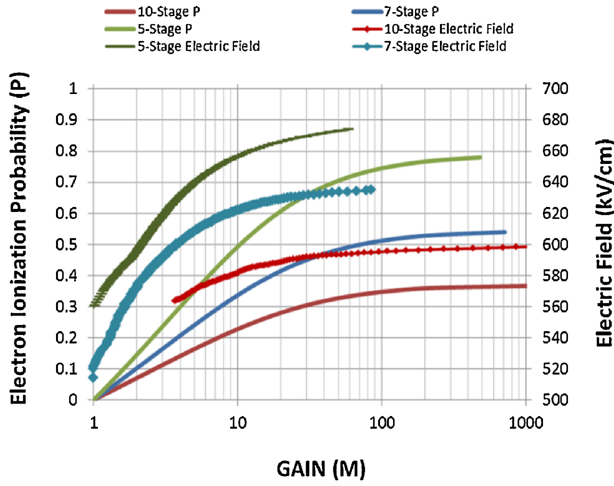

Fig. 9. Probability of Electron Ionization Per Stage from (7; $k_s = 0.036$) as a function of gain and the electric field estimated from the I-V curves using the band edge modeler.

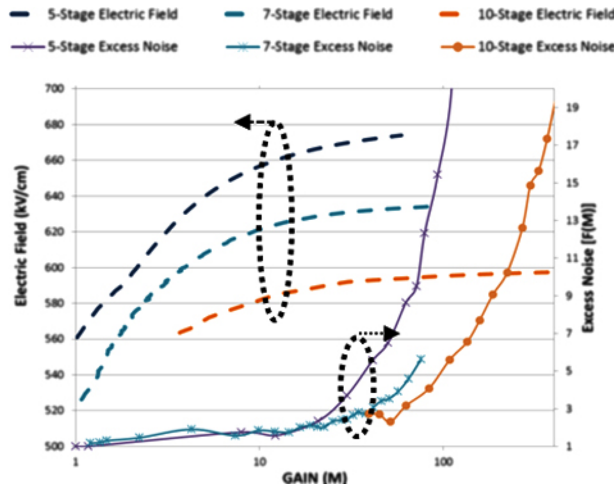

Fig. 10. The electric field estimated by the band edge modeler as a function of output gain level for each number gain stage SCM APD. Also plotted is the measured excess noise for each device.

measured at each bias. For example, for a 7-stage device, at gain of $M_{DC} = 42$, where the 7-stage data deviates from (9; $k_s = 0.036$), carrier probabilities of $P = 0.47$ and $Q = 0.02$ can be calculated from (10; $k_s = 0.036$). For a 5-stage device, these same carrier ionization probabilities would result in a gain of about $M_{DC} = 9$, whereas for these same carrier ionization probabilities a 10-stage SCM APD would be in avalanche breakdown.

Similarly, the data in Fig. 9 show that for any M_{DC}, a 10-stage device operates with a lower electric field than the 7- and 5-stage devices. For example, for $M_{DC} = 42$, the electric field of the 10-stage SCM APD is 595 kV/cm; whereas the 7-stage and 5-stage devices are 636 kV/cm and 676 kV/cm respectively. This is expected, as less gain is needed in each stage as the number of gain stages in the multiplication region increases.

A lower electric field is important because it reduces the magnitude of the electric field-dependent trap-assisted-tunneling dark current [44]. The relationship between electric field and dark current generation in the various SCM APDs

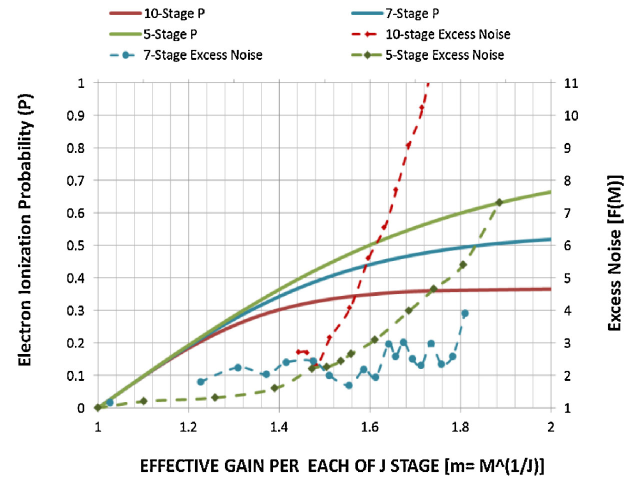

Fig. 11. Measured excess noise and the electron ionization probability, P, calculated from (10) plotted as a function of the effective gain per stage ($m_{eff} = <M_{DC}>^{1/J}$).

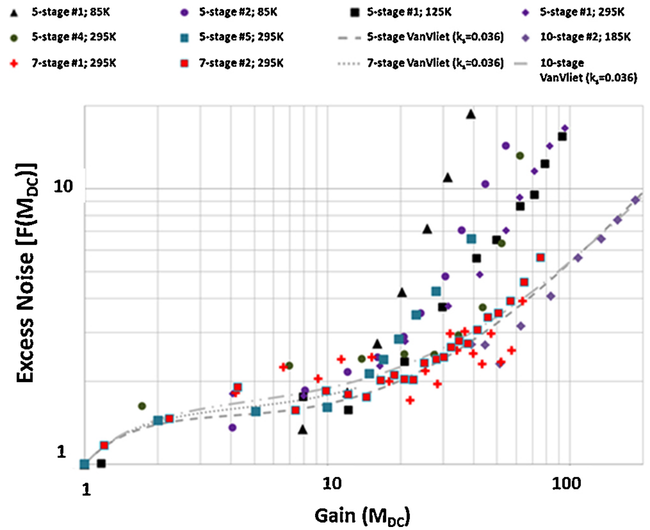

Fig. 12. Plot of 5-stage SCM APDs measured at various temperatures, shown alongside the measured excess noise data from two 7-stage devices and a 10-stage device. Also shown for reference is (9; $k_s = 0.036$) plotted for each number of gain stages.

is illustrated in Fig. 6. The I-V curves show that at any M_{DC}, the 10-stage SCM APDs operate with lower dark currents than the devices with fewer gain stages.

To elucidate the effects of the electric field on the multi-stage SCM APDs, the electric field and excess noise are plotted in Fig. 10 as a function of output gain. For an excess noise of $F(M_{DC}) = 3$, Fig. 10 shows that the 5-, 7-, and 10-stage devices are operated with electric fields of 670, 635, and 595 kV/cm, respectively, and from Fig. 9 we can determine that operating under these electric fields, $P \approx 0.7$, 0.5, and 0.36, respectively. The data illustrate, for each of the various numbered gain stages, the electric fields needed to achieve specific P and Q values and show the impact the SCM APD design has on M_{DC} and $F(M_{DC})$.

The plots of Fig. 11 help to illustrate further the interplay between the number of gain stages and the electric field dependent carrier ionization probabilities on the gain and excess noise resulting from ionization feedback.

In Fig. 11, the estimated electron ionization probabilities from (10; $k_s = 0.036$) and the measured excess noise values are plotted as a function of the average effective gain per stage, calculated assuming that all of the SCM APD gain occurs without ionization feedback; the effective gain for each stage is calculated using $m_{eff} = <M_{DC}>^{1/J}$. It is interesting to note that in Fig. 11, the excess noise data do not occur in the same order as the number of gain stages. For example, at $F(M_{DC}) = 3$, the 7-stage device is operating at an effective gain per stage of about $m_{eff} = 1.8$, whereas the 5-stage device is operating at $m_{eff} = 1.6$, and the 10-stage $m_{eff} = 1.5$. This result illustrates the effect of carrier ionization probabilities (increased electric fields) and the number of gain stages on the DC gain and excess noise. It also demonstrates that as the number of gain stages increases, small increases in hole ionization feedback can have significant impact on the gain and excess noise of the SCM APD.

3) *Higher Gain Per Stage/Higher Feedback "Bulk-like" Multiplication:* When the bias is increased to higher output gain levels, P and Q continue to increase in proportion to one another, and with a sufficient number of gain stages to support ionization feedback, the excess noise models for bulk semiconductor multiplication regions [i.e., (4)] can be applied to the SCM APD. Only the 10-stage device has a sufficient number of gain stages for these conditions to apply. For the 10-stage SCM APDs, the measured data can be approximated by (4; $k = 0.036$) above $M_{DC} \approx 125$. Using (10; $k_s = 0.036$), at this gain, $P = 0.35$. At this same electron ionization probability, using (10; $k_s = 0.036$), the 5- and 7-stage devices have DC gains of $M_{DC} = 5.14$ and $M_{DC} = 11.58$, respectively.

4) *Increased Multiplication Approaching Breakdown due to Increased Hole Feedback:* At even higher biases, P and Q increase sufficiently for ionization feedback effects to dominate excess noise performance as the devices approach avalanche breakdown. The 5-stage SCM APD deviates from (9; $k_s = 0.036$) at $M_{DC} \approx 14$ and the 7-stage device at $M_{DC} \approx 42$. From (10; $k_s = 0.036$), we can calculate that at these output gain values, $P = 0.6$ for the 5-stage SCM APD and $P = 0.47$ for the 7-stage device.

5) *Avalanche Breakdown:* At higher biases, the 5-stage and 7-stage SCM APDs experience avalanche breakdown, whereas, the 10-stage SCM APDs do not. The lack of breakdown in the 10-stage devices is indicative of single carrier (electron) dominated ionization.

B. Performance Variability

The published literature lacks carrier impact-ionization rate data for the quaternary alloy $Al_{0.335}Ga_{0.140}In_{0.525}As$ over the range of electric fields and operating temperatures in which the SCM APD is operated, preventing direct Monte Carlo or numeric modeling of temperature effects.

To test the effects of temperature and process variability on the SCM APD performance, 5-stage SCM APDs were tested over a range of temperatures. Fig. 12 plots this data alongside data for two 7-stage devices tested at 295K and the 10-stage SCM APD device tested at 185K. All of the data show good approximation to (9; $k_s = 0.036$) over the expected gain ranges, and the deviation of the 5-stage SCM APD data from (9; $k_s = 0.036$) at about $M_{DC} = 13$ ($P = 0.54$) is consistent between devices over the range of temperatures. While some measurement variability is present, the overlap of the various device performances at low gains indicates good calibration in the measurements.

There is some indication in the 5-stage SCM APD data that at lower temperatures, avalanche breakdown may occur at a faster rate than the higher operating temperatures. This may be a result of reduced phonon scattering of holes in the "cool down" region of the gain stages (Fig. 2, inset label iii) at low temperatures, leading to increased hole ionization feedback effects as bias is increased.

VIII. CONCLUSION

The multi-stage InGaAs/InAlAs SCM APD designs were shown to operate at high linear-mode gain with low excess noise. The SCM APD's cascaded series of asymmetric multiplication stages employ variations of alloy composition, layer thickness, and doping to modulate carrier energy and associated dead space inside the junction, maximizing electron-initiated impact ionization while minimizing hole ionization.

The SCM APD design has been analyzed using Monte Carlo and numerical simulations, which were in good agreement. The designs were empirically validated through growth, fabrication, and test of multiple implementations. The performance of the devices was shown to be approximated by analytical models previously developed for discrete gain stage "staircase" and low ionization feedback "superlattice" APDs.

At equivalent output signal gains, the SCM APDs with more multiplication stages were shown to display lower excess noise and lower dark current than those devices with a lower number of gain stages. Select 10-stage devices exhibited gains exceeding 6 000, with an excess noise characterized by $k < 0.04$ for $150 < M_{DC} < 1300$, and with sub-McIntyre performance, i.e., (4, $k = 0.036$) at gains up to about $M_{DC} = 125$.

This level of room temperature gain with low excess noise exceeds that of known InGaAs and HgCdTe APD published results, making the innovation promising for a range of scientific, communications, and military applications requiring compact, robust, linear short-wave infrared (SWIR) photo detectors with high internal gain.

Anticipated future test measurements will investigate the instantaneous (time-resolved) gain and noise characteristics of the device. Future SCM APD design improvements will include excess noise reductions through refinement of the gain stage architecture, dark current reduction, implementation in other semiconductor alloy systems such as InGaAs/InP and GaAs/AlGaAs, and implementation with a larger number of multiplying stages. Suitably fabricated, devices with a larger number of gain stages are expected to have still higher gain and lower excess noise, with the tradeoff of increased junction transit time and concomitant lower bandwidth.

REFERENCES

[1] P. Bhattacharya, *Semiconductor Optoelectronic Devices, 2*nd ed., NJ, USA: Prentice Hall, 1997, p. 384.
[2] R. J. McIntyre, "The distribution of gains in uniformly multiplying avalanche photodiodes: Theory," *IEEE Trans. Electron. Devices*, vol. 19, no. 6, pp. 703–713, Jun. 1972.

[3] R. E. Burgess, "Homophase and heterophase fluctuations in semiconducting crystals," in *Proc. Discussions Faraday Soc.*, vol. 28. pp. 151–158, 1959.

[4] R. E. Burgess, "Some topics in the fluctuations of photo-processes in solids," *J. Phys. Chem. Solids*, vol. 22, pp. 371–377, Dec. 1961.

[5] M. C. Teich, K. Matsuo, and B. E. A. Saleh, "Excess noise factors for conventional and superlattice avalanche photodiodes and photomultiplier tubes," *IEEE J. Quantum Electron.*, vol. 22, no. 8, pp. 1184–1193, Aug. 1986.

[6] R. J. McIntyre, "Multiplication noise in uniform avalanche diodes," *IEEE Trans. Electron. Devices*, vol. 13, pp. 164–168, Jan. 1966.

[7] K. A. Anselm, P. Yuan, C. Hu, C. Lenox, H. Nie, G. Kinsey, J. C. Campbell, and B. G. Streetman, "Characteristics of GaAs and AlGaAshomo junction avalanche photodiodes with thin multiplication regions," *Appl. Phys. Lett.*, vol. 71, no. 26, pp. 3883–3885, Dec. 1997.

[8] C. Lennox, P. Yuan, H. Nie, O. Bakelov, C. Hansing, J. C. Campbell, A. L. Holmes, Jr., and B. G. Streetman, "Thin multiplication region InAlAshomojunction avalanche photodiodes," *Appl. Phys. Lett.*, vol. 73, no. 6, pp. 783–784, Aug. 1998.

[9] M. A. Saleh, M. M. Hayat, B. E. A. Saleh, and M. C. Teich, "Dead-space-based theory correctly predicts excess noise factor for thin GaAs and AlGaAs avalanche photodiodes," *IEEE Trans. Electron. Devices*, vol. 47, no. 3, pp. 625–633, Mar. 2000.

[10] C. H. Tan, J. P. R. David, G. J. Rees, R. C. Tozer, and D. C. Herbert, "Treatment of soft threshold in impactionization," *J. Appl. Phys.*, vol. 90, no. 5, pp. 2538–2543, Sep. 2001.

[11] S. Wang, R. Sidhu, X. G. Zheng, X. Li, X. Sun, A. L. Holmes, Jr., and J. C. Campbell, "Low-noise avalanche photodiodes with graded impact-ionization-engineered multiplication region," *IEEE Photon. Technol. Lett.*, vol. 13, no. 12, pp. 1346–1348, Dec. 2001.

[12] M. M. Hayat, O.-H. Kwon, S. Wang, J. C. Campbell, B. E. A. Saleh, and M. C. Teich, "Boundary effects on multiplication noise in thin heterostructure avalanche photodiodes: Theory and experiment," *IEEE Trans. Electron. Devices*, vol. 49, no. 12, pp. 2114–2123, Dec. 2002.

[13] S. Wang, J. B. Hurst, F. Ma, R. Sidhu, X. Sun, X. G. Zheng, A. L. Holmes, Jr., A. Huntington, L. A. Coldren, and J. C. Campbell, "Low-noise impact-ionization-engineered avalanche photodiodes grown on InP substrates," *IEEE Photon. Technol. Lett.*, vol. 14, no. 12, pp. 1722–1724, Dec. 2002.

[14] S. Wang, F. Ma, X. Li, R. Sidhu, X. Zheng, X. Sun, A. L. Holmes, Jr., and J. C. Campbell, "Ultra-low noise avalanche photodiodes with a 'centered-well' multiplication region," *IEEE J. Quantum Electron.*, vol. 39, no. 2, pp. 375–378, Feb. 2003.

[15] O.-H. Kwon, M. M. Hayat, S. Wang, J. C. Campbell, A. Holmes, Jr., Y. Pan, B. E. A. Saleh, and M. C. Teich, "Optimal excess noise reduction in thin heterojunction $Al_{0.6}Ga_{0.4}$As-GaAs avalanche photodiodes," *IEEE J. Quantum Electron.*, vol. 39, no.10, pp. 1287–1296, Oct. 2003.

[16] C. Groves, J. P. R. David, G. J. Rees, and D. S. Ong, "Modeling of avalanche multiplication and noise in heterojunction avalanche photodiodes," *J. Appl. Phys.*, vol. 95, no. 11, pp. 6245–6251, Jun. 2004.

[17] C. Vèrié, F. Raymond, J. Besson, and T. Nguyen Duy, "Bandgap spin-orbit splitting resonance effects in Hg1-xCdxTe alloys," *J. Crystal Growth*, vol. 59, nos. 1–2, pp. 342–346, Sep. 1982.

[18] B. Orsal, R. Alabedra, M. Valenza, G. Lecoy, J. Meslage, and C. Y. Boisrobert, "$Hg_{0.4}Cd_{0.6}$Te 1.55-μmavalanche photodiode noise analysis in the vicinity of resonant impact ionization connected with the spin-orbit split-off band," *IEEE Trans. Electron. Devices*, vol. 35, no. 1, pp. 101–107, Jan. 1988.

[19] K. A. El-Rub, C. H. Grein, M. E. Flatte, and H. Ehrenreich, "Band structure engineering of superlattice-based short-, mid-, and long-wavelength infrared avalanche photodiodes for improved impact ionization rates," *J. Appl. Phys.*, vol. 92, no. 7, pp. 3771–3777, Oct. 2002.

[20] F. Ma, X. Li, J. C. Campbell, J. D. Beck, C.-F. Wan, and M. A. Kinch, "Monte Carlo simulations of HgCdTe avalanche photodiodes and resonance phenomenon in the multiplication noise," *Appl. Phys. Lett.*, vol. 83, no. 4, pp. 785–787, Jul. 2003.

[21] M. A. Kinch, J. D. Beck, C.-F. Wan, F. Ma, and J. Campbell, "HgCdTe avalanche photodiodes," *J. Electron. Mater.,* vol. 33, pp. 630–639, Jun. 2004.

[22] A. R. J. Marshall, C. H. Tan, M. J. Steer, and J. P. R. David, "Extremely low excess noise in InAs electron avalanche photodiodes," *IEEE Photon. Technol. Lett.*, vol. 21, no. 13, pp. 866–868, Jul. 2009.

[23] P. Yuan, S. Wang, X. Sun, X. G. Zheng, A. L. Holmes, Jr., and J. C. Campbell, "Avalanche photodiodes with an impact-ionization-engineered multiplication region," *IEEE Photon. Technol. Lett.*, vol. 12, no. 10, pp. 1370–1372, Oct. 2000.

[24] B. E. A. Saleh, M. M. Hayat, and M. C. Teich, "Effect of dead space on the excess noise factor and time response of avalanche photodiodes," *IEEE Trans. Electron. Devices*, vol. 37, no. 9, pp. 1976–1984, Sep. 1990.

[25] P. Yuan, K. A. Anselm, C. Hu, H. Nie, C. Lenox, A. L. Holmes, B. G. Streetman, J. C. Campbell, and R. J. McIntyre, "A new look at impact ionization–Part II: Gain and noise in short avalanche photodiodes," *IEEE Trans. Electron. Devices*, vol. 46, no. 8, pp. 1632–1639, Aug. 1999.

[26] K. F. Li, S. A. Plimmer, J. P. R. David, R. C. Tozer, G. J. Rees, P. N. Robson, C. C. Button, and J. C. Clark, "Low avalanche noise characteristics in thin InP p/sup + /-i-n/sup + / diodes with electron initiated multiplication," *IEEE Photon. Technol. Lett.*, vol. 11, no. 3, pp. 364–366, Mar. 1999.

[27] O.-H. Kwon, M. M. Hayat, J.C. Campbell, B. E. A. Saleh, M.C. Teich, "Effect of stochastic dead space on noise in avalanche photodiodes,"*IEEE Trans. Electron Devices*,vol. 51, no. 5, pp. 693–700, May 2004.

[28] P. Yuan, H. Chad, K. A. Anselm, C. Lenox, H. Nie, H. L. Holmes, B. G. Streetman, and J. C. Campbell, "Impact ionization characteristics of III-V semiconductors for a wide range of multiplication region thicknesses," *IEEE J. Quantum Electron.*, vol. 36, no. 2, pp. 198–204, Feb. 2000.

[29] S. Wang, F. Ma, X. Li, R. Sidhu, X. Zheng, X. Sun, A. L. Holmes, Jr., and J. C. Campbell, "Ultra-low noise avalanche photodiodes with a centered-well multiplication region," *IEEE. J. Quantum Electron.*, vol. 39, no. 2, pp. 375–378, Feb. 2003.

[30] G. M. Williams, D. A Ramirez, M. M. Hayat, and A. S. Huntington, "Time resolved gain and excess noise properties of InGaAs/InAlAs avalanche photodiodes with cascaded discrete gain layer multiplication regions," *J Appl. Phys.*, vol. 113, no. 9, p. 093705, Mar. 2013.

[31] A. Huntington, *United States Patent* 7,432,537, 2008.

[32] G. F. Williams, F. Capasso, and W. T. Tsang, "The graded bandgap multilayer avalanche photodiode: A new low-noise detector," *IEEE Electron Device Lett.*, vol. 3, no. 3, pp. 71–73, Mar. 1982.

[33] M. A. Saleh, M. M. Hayat, O.-H. Kwon, A. L. Holmes, Jr., J. C. Campbell, B. E. A. Saleh, and M. C. Teich, "Breakdown voltage in thin III–V avalanche photodiodes,".*Appl. Phys. Lett.*, vol. 79, no. 24, pp. 4037–4039, Dec. 2001.

[34] M. A. Saleh, M. M. Hayat, B. E. A. Saleh, and M. C. Teich, "Dead-space-based theory correctly predicts excess noise factor for thin GaAs and AlGaAs avalanche photodiodes," *IEEE Trans. Electron. Devices*, vol. 47, no. 3, pp. 625–633, Mar. 2000.

[35] T. P. Pearsall, "Impact ionization rates for electrons and holes in Ga0.47In0.53As," *Appl. Phys. Lett.*, vol. 36, no. 3, pp. 218–220, Feb. 1980.

[36] F. Osaka, T. Mikawa, and T. Kaneda, "Impact ionization coefficients of electrons and holes in (100)-oriented $Ga_{1-x}In_xAs_yP_{1-y}$," *IEEE J. Quantum Electron.*, vol. 21, pp. 1326–1338, Sep. 1985.

[37] M. M. Hayat, B. E. A. Saleh, and M. C. Teich, "Effect of dead space on gain and noise of double-carrier-multiplication avalanche photodiodes," *IEEE Trans. Electron. Devices*, vol. 39, no. 3, pp. 546–552, Mar. 1992.

[38] J. P. R. David, J. Allma, A. R. Adams, J. S. Roberts, R. Grey, G. J. Rees, and P. N. Robson, "Avalanche breakdown in AlxGa1-xAs alloys and Al0.3Ga0.7As/GaAs multilayers," *Appl. Phys. Lett.*, vol. 66, no. 21, pp. 2876–2878, May 1995.

[39] F. Capasso, W. T. Tsang, and G. F. Williams, "Staircase solid-state photomultipliers and avalanche photodiodes with enhanced ionization rates ratio," *IEEE. Trans. Electron. Devices*, vol. 30, no. 4, pp. 381–390, Apr. 1983.

[40] K. M. van Vliet, A. Friedmann, and L. M. Rucker, "Theory of carrier multiplication and noise in avalanche devices–Part II: Two-carrier processes," *IEEE Trans. Electron. Devices*, vol. 26, no. 5, pp. 752–764, May 1979.

[41] W. A. Lukaszek, A. van der Ziel, and E. R. Chenette, "Investigation of the transition from tunneling to impact ionization multiplication in silicon *p-n* junctions," *Solid-State Electron.*, vol. 19, no. 1, p. 57, Jan. 1976.

[42] M. C. Teich, K. Matsuo, and B.E.A. Saleh, "Excess noise factors for conventional and superlattice avalanche photodiodes and photomultiplier tubes," *IEEE J. Quantum Electron.*, vol. 22, no. 8, pp. 1184–1193, Aug. 1986.

[43] B. E. A. Saleh, M. M. Hayat, and M. C. Teich, "Effect of dead space on the excess noise factor and time response of avalanche photodiodes," *IEEE Trans. Electron. Devices*, vol. 37, no. 9, pp. 1976–1984, Sep. 1990.

[44] S. R. Forrest, "Performance of InxGa1-xAsyP1-yphotodiodes with dark current limited by diffusion, generation recombination, and tunneling," *IEEE J. Quantum Electron.*, vol. 17, no. 2, pp. 217–226, Feb. 1981.